Journal of Energy Storage 55 (2022) 105677

Contents lists available at ScienceDirect

Journal of Energy Storage

journal homepage: www.elsevier.com/locate/est

Research papers

Effect of processing on microstructure and mechanical properties of pentaglycerine based solid-solid phase change materials

Angel Serrano [a,*], Ignacio Garrido [b,c], Sergio Santos [a,d,e], Mikel Duran [a,f], Jean-Luc Dauvergne [a], Manuel Carmona [b], Elena Palomo Del Barrio [a,g]

[a] Centre for Cooperative Research on Alternative Energies (CIC energiGUNE), Basque Research and Technology Alliance (BRTA), Alava Technology Park, Albert Einstein 48, 01510 Vitoria-Gasteiz, Spain
[b] Institute of Chemical and Environmental Technologies, Department of Chemical Engineering, University of Castilla – La Mancha, Av. Camilo José Cela s/n, 13004 Ciudad Real, Spain
[c] School of Architecture, Department of Mechanical Engineering, University of Castilla – La Mancha, Avenida Carlos III s/n, 45071 Toledo, Spain
[d] TECNALIA, Basque Research and Technology Alliance (BRTA), Parque Tecnológico de San Sebastián, 20009 Donostia-San Sebastián, Spain
[e] Applied Physics, University of the Basque Country (UPV/EHU), 48940 Leioa, Spain
[f] Chemical and Environmental Engineering Department, University of the Basque Country (UPV/EHU), Plaza Europa 1, 20018 Donostia-San Sebastián, Spain
[g] Ikerbasque, Basque Foundation for Science, 48013 Bilbao, Spain

ARTICLE INFO

Keywords:
Solid-solid phase change material
Plastic crystal
Pentaglycerine
Expanded graphite
Processing

ABSTRACT

The present work addresses the lack of reported information about the mechanical properties of solid-solid PCMs, and how these are affected by their processing, considering that they usually incorporate fillers to increase their thermal conductivity. To this end, this work analyzes pentaglycerine (PG) based composites, which are of great interest in TES intended for 80 °C. These composites are also doped with various contents of expanded graphite (EG) with two different particle sizes. With these combinations, the effect of two typical processing methods, pressing and casting, on the microstructure of the composites is evaluated. Furthermore, the mechanical behavior of these composites in both crystal and plastic phases, as well as their thermal expansion during the transition process, is also reported in the current study. Besides demonstrating the important role that processing plays in these properties in PG/EG-based composites, it has been found that the use of EG is also beneficial for mitigating the permanent deformations experienced by these composites during thermal cycling. Finally, the exposed results give the first evidence of the interesting effect these processing methods have on the thermal properties of the composites.

1. Introduction

Phase change materials (PCMs) store a large amount of thermal energy (as latent heat) thanks to their phase changes (solid-liquid or solid-solid) while maintaining an almost constant temperature during the transition process [1]. These systems offer a much higher storage density within a narrower temperature range than those based on sensible heat, such as water tanks. In this regard, employing PCMs undergoing solid phase transitions (solid-solid PCMs) can be an attractive alternative to achieve TES compactness while avoiding the cost related to heat exchangers or PCM macro-encapsulation, that account for c.a. 70 % of the total cost of the TES system is many cases. Plastic crystals are one of these particular PCMs with solid-solid transitions that generate significant interest in the energy storage community. These molecules undergo reversible solid phase transitions from a low temperature ordered structure, denoted as crystal phase, to a high temperature orientationally disordered phase, also known as plastic phase. Their transition temperatures range from 30 °C to 190 °C, with unusually high latent heat, and their binary and ternary mixtures give rise to new solid PCMs with "on-demand" energy storage properties. The possibility of easily adapting the working temperature confers to these composites the versatility requested by the market [2–4].

Concerning these materials, extensive work has been reported on the characterization and enhancement of their thermal properties. Some works have even evaluated the performance of these materials in TES demonstration applications, but they have mainly employed macro-encapsulation through a shell and tube heat exchanger, not making use of the advantages of a solid-solid PCM [5,6].

* Corresponding author.
E-mail address: aserrano@cicenergigune.com (A. Serrano).

https://doi.org/10.1016/j.est.2022.105677
Received 30 May 2022; Received in revised form 11 August 2022; Accepted 13 September 2022

Regarding the thermal properties of these materials, mainly the solid-solid transitions of neopentylglycol (NPG), pentaglycerine (PG), and pentaerythritol (PE) have been studied, focusing on the specific heats, transition temperatures, and latent heats, as well as on the understanding of these transitions of both pure materials and their binary and ternary systems [7–15]. Like in most PCMs, a great deal of work has been done on these materials to improve their thermal properties and, overall, their thermal conductivities. Examples of this thermal conductivity enhancement applied to plastic crystals can be found in PE, whose transition temperature of 180 °C makes it ideal for industrial applications. In this line, various studies have been done analyzing the effect of both alumina particles and copper nanoparticles on the energy performance of PE-based composites [16–18]. The latest reported studies on PE appear to be aimed at using carbon-based materials, such as graphene. Hence, T. Liu et al. doped PE with graphene powders reaching contents up to 3 wt% [19]. By comparing the effect of graphene with alumina particles, they concluded that, due to the increase of carbon atom spacing in graphene, the interaction between graphene and pentaerythritol is enhanced and the heat transfer is further facilitated. Indeed, carbon-based materials are among the most widely used doping agents to increase PCMs thermal conductivity. Hence, trying to avoid PCM leakage, D.J. Johnson et al. [20] injected PG in graphite foams by forcing the melted PCM to flow through the foam with sufficient mass flow and pressure to displace trapped air, allowing the PCM to occupy up to 75 % of the available pore volume. Even so, the PCM content in the final composite is low, around 40 wt%, with a consequent loss of thermal storage capacity. Adding a small percentage of particles remains the most promising strategy to avoid noticeable latent heat loss. Thereby, N. Zhang et al. [21] developed a new PG-based solid-solid PCM by doping with expanded graphite. They employed up to 4 wt% EG, achieving a thermal conductivity of 0.944 W/m·K (in contrast to 0.35 W/m·K for the raw PG [22]). To fabricate these composites, they performed a first homogenization treatment by ball milling, followed by a complete melting of the PG at 300 °C and a further cooling down to obtain the final piece.

As can be noticed, although they are composites that are proposed to be used in their solid-state, current literature focuses on their thermophysical properties, but it does not provide adequate information on their mechanical properties and shape stability at different temperatures. Nor on the effect of processing on their properties, although it directly affects the composite structure. And this affirmation can be applied not only to plastic crystals but also to the great majority of solid-solid PCMs [23–26]. The great interest of solid-solid PCMs lies in the possibility of using them directly in the TES system without the need for encapsulation or heat exchangers, so understanding the behavior of these materials under mechanical stress in both crystalline phases is crucial to extract their full potential, or to tackle and correct those weak points likely to appear during thermal cycling.

The present work addresses this aspect of solid-solid PCMs, evaluating their mechanical behavior both at high and low temperatures, therefore, in their two crystalline phases involved in the energy storage process. For this purpose, we focus on Pentaglycerine (PG), whose transition temperature at 80 °C and latent heat of 175 J/g are especially interesting in applications such as solar heating and district heat water (DHW) production. Considering that doping agents are generally used to improve the PCM thermal conductivity, the addition of different amounts of expanded graphite with two different particle sizes is evaluated since these additives affect the mechanical behavior of the composites. Composite processing also affects the mechanical behavior of composites, since it modifies the microstructure of the composite, and therefore playing a relevant role in the final performance of the system. Hence, two standard processing are going to be tested: casting, which is the one that predominates in the literature when dealing with these materials; and pressing, due to its simplicity, low cost [27], and high performance to obtain pieces to fill, for example, a tank of a TES system. The microstructure of the composite is directly responsible for the mechanical behavior, so we start with a detailed characterization of the microstructure, trying to understand the effect of processing and doping in the formation of this microstructure. Finally, thermal expansion, an important parameter when dealing with phase change composites stacked or confined in a tank, is also analyzed.

2. Materials and methods

2.1. Materials

1,1,1-Tris(hydroxymethyl)ethane (purity 98 %) supplied by Sigma-Aldrich, also known interchangeably as pentaglycerine (PG) or trimethylolethane, was selected as solid-solid PCM. PG exhibits a tetragonal crystal phase at low temperature and a face-centered cubic (FCC) crystal structure at high temperature. The enthalpy of transition is 192 J/g, which takes place at 81 °C for the crystal-plastic transition, meanwhile the plastic-crystal transition has been reported at 74–68 °C [7,12,20,21], therefore, PG exhibits subcooling. On the other hand, highly conductive expanded graphite powder, SIGRATHERM®GFG, supplied by SGL Carbon, was used as additive for this solid-solid PCM. Two different expanded graphite particle sizes were used, 75 μm and 600 μm, hereinafter referred to as EG_{75} and EG_{600}, respectively.

2.2. Composite processing methods. Devices and elaboration process

Two main processing methods were tested: uniaxial cold pressing and casting. The processing effect has been studied in both bare PG and PG doped with two different expanded graphite (EG_{75} and EG_{600}). The EG content added in both processing methods were 0, 1, 5, and 10 wt%.

- In the uniaxial pressing, the PCM in powder was compacted in a metal die by the pressure applied in a single direction. This method is confined to relatively simple shapes; however, production rates are high, and the process is inexpensive [28]. A hydraulic manual press from Specac Ltd. (Atlas Manual Press 15 T) has been used for the uniaxial cold pressing. The selected mold for the pellet preparation was made of stainless steel, having a cylindrical shape of 13 mm in diameter. For the elaboration of the pellets the PG was initially subjected to a ball milling process for 15 min using a Spex mixer mill (Spex sampleprep) with stainless steel vials and stainless-steel balls under mild conditions (3 balls of 3 mm with a ball powder ratio (BPR) = 1). The addition of expanded graphite was carried out after the PG milling process, avoiding modifying the initial particle size of expanded graphite during the milling. Next, the PG-EG mixture was manually homogenized, and the obtained powder was poured into the die cavity. The powder was then compacted by means of pressure applied to the top die (370 MPa during 30 s), and the compacted piece was ejected by the rising action of the bottom punch.
- For the casting method, in an initial stage, two different solidification rates have been tested in bare PG to select the proper one for elaborating the composites, fast and slow cooling:
  - For fast cooling (4 °C/min), the device consists of a cylindrical tube made with cooper to increase the heat transfer between the composite and its environment. The diameter of the mold used in fast cooling was considerably smaller than that used for slow cooling to speed up the solidification. The heating was done with a hot plate at the base of the cylinder while to promote the fast-cooling rate, the solidification was carried out by free cooling at room temperature, reaching a cooling rate of 4 °C/min.
  - In the slow casting (0.5 °C/min), the sample was deposited on a glass container which was then placed inside a sealed stainless-steel reactor and melted in an oven. For the solidification step, the oven was switched off allowing the sample to cool down slowly at 0.5 °C/min inside the oven to room temperature.

From this initial analysis in bare PG and based on the obtained

microstructure, only one solidification rate was selected to manufacture the doped samples by casting. The procedure was similar independently of the cooling rate. The PG was incorporated as received (in powder) in the casting device and melted at 210 °C, followed by the solidification step previously detailed according to fast or slow casting. The expanded graphite was incorporated by manual stirring during the melting process of the material, ensuring homogenization of the mixture before solidification.

The nomenclature used hereafter to identify the different samples is specified as $XWEG_Y$, where X is the processing and can be P for pressing or C for casting; W refers to the weight percentage of added expanded graphite; and EG_Y is the type of expanded graphite (EG_{75} or EG_{600}). When referring to a complete series of composites rather than specific percentages of graphite, the symbol "_" is used. Therefore, a composite elaborated by casting with a 5 wt% of EG_{600} is denoted as $C5EG_{600}$, and all the set of composites elaborated by casting and EG_{600} is denoted as C_EG_{600}.

2.3. Characterization

2.3.1. Microstructure

To analyze their microstructure, the samples were imaged using a scanning electron microscope Quanta 200 FEG operated in low vacuum mode at 10 kV featured with a backscattered electron detector (BSED) and large field low vacuum detector (LFD). The operational conditions were carefully selected to avoid the melting of PG during the study. The average grain size was determined from SEM pictures by using the software ImageJ2.0 [29] and the linear intercept technique [30]. Various random straight lines are randomly drawn through the micrograph in this method. Then, the number of grain boundaries intersecting the line is counted. The average grain size is found by dividing the total actual length of all the lines by the number of counted intersections. The grain size was measured directly on the image in cases where the porosity of the sample or the presence of diffuse edges hampers the use of the linear intercept technique.

2.3.2. True and bulk density

The true density (ρ_{true}) of the composites was determined by helium pycnometer Micromeritics Accupyc 1340 at room temperature. The dimensions (diameter and height) and mass of three cylindrical probes for each sample were measured and used to determine the bulk density (ρ_{bulk}). The porosity of the composites (ε) was estimated from the bulk density, the true density, and assuming that the sample pores are filled with air (Eq. (1)). The air density was considered 1.186 kg/m^3, corresponding to the density under normal conditions.

$$\varepsilon = \frac{\rho_{true} - \rho_{bulk}}{\rho_{true} - \rho_{air}} \quad (1)$$

2.3.3. Mechanical properties

The mechanical properties of the samples were analyzed through uniaxial compression tests using a MTS 370.02 testing instrument. The compression tests were carried out at a 0.5 mm/min cross-head speed. The dimensions of each tested specimen (cylinders) were registered, and each analysis was repeated 3 times. The analysis was carried out at two different temperatures, at room temperature (crystal phase) and 120 °C (plastic phase). From these test results, the specific modulus (E*), which is the Young's modulus per mass density of a material, was determined as the slope value of the initial part of the compression curves divided by the apparent density, while the yield point is determined using the 0.002 strain offset method.

2.3.4. Thermal expansion

The dimensional changes versus temperature and time both during the phase transition and upon the heating and cooling were measured in a DIL 402 C/4/G pushrod dilatometer from NETZSCH. This equipment was used to determine the thermal expansion of the samples by setting a dynamic heating and cooling rate of 0.8 °C/min from 40 °C to 120 °C in a controlled nitrogen flow of 100 mL/min. The obtained results were compared to those obtained from Differential scanning calorimetry (DSC) was used to determine the transition temperatures of the composites. For the cycling test, the heating/cooling rate was set at 2 °C/min to accelerate the analysis.

3. Results

3.1. Morphology and inner structure

3.1.1. Bare PG

Uniaxial cold pressing and casting were used for the processing of bare PG. Initially, the two different solidification rates (fast and slow) were tested to determine their effect on the PG microstructure.

Fig. 1 provides details of the microstructure along the radial axis of the cast sample PG processed at a fast cooling rate. In these images, two main zones can be easily identified, the chill zone and the columnar zone, both characteristic elements of casting. The chill zone, composed of dense and fine grain structure, is visible at the edge of the probe, where the solidification process starts since the heat dissipation is faster at the mold surface. The columnar zone contains elongated grains that grow along the radial axis to the center of the probe. This direction of growth is opposite to the heat flow, from the coldest to the hottest area of the casting. If we examine the middle zone closely, we can notice that these columnar grains are composed of many dendrites with an interdendritic distance between 2 and 10 μm. The appearance of these dendrites indicates that the molten PG is undercooled before any nucleation takes place to promote solidification.

Two defects are visible in the microstructure due to shrinkage during the solidification process. On the one hand, an interdendritic shrinkage or interdendritic porosity is visible between the columnar grains. On the other hand, a large shrinkage cavity appears at the center of the sample. This cavity is even visible in the picture of the probe (Fig. 1.a) and occurs when one zone solidifies slower than the others (center slower than the mold wall). The scheme depicted in Fig. 1.d helps to understand the different elements that can be identified.

Fig. 2.a and b shows the SEM images of cast PG processed at a slow cooling rate. The images reveal the presence of the chill grains at the edge of the sample, followed by thick columnar grains. It is noteworthy that the dendrite size is larger than that observed in fast cooling, with an interdendritic distance up to 10 times larger (60–120 μm) than in the previous case. This shows that the cooling rate affects the size of the dendrites. The distance between secondary dendritic branches is reduced when the casting is cooled faster, as a thinner dendritic network conducts the heat from the solidified part to the subcooled liquid more efficiently. As in the previous sample, shrinkage porosity is observed; however, as there are no significant temperature gradients in the piece during solidification, the presence of a shrinkage cavity is avoided.

Although shorter secondary dendritic arm distances are related to higher mechanical strengths [31], the formation of a shrinkage cavity, which can strongly affects the mechanical stability of the composite, forces us to select a slow cooling rate to carry out the addition of expanded graphite in further castings.

In contrast to casting, uniaxial pressing produces pieces with a more homogeneous structure, free of significant defects resulting from shrinkage (Fig. 2.c). A higher magnification (Fig. 2.d) reveals the distribution of the small PG crystals, with an average grain size of 1.75 μm. Although, as we have mentioned, the structure is free of large defects, some small cavities typical of the compaction processes can be observed, which give rise to slight porosities in the final piece.

3.1.2. Expanded graphite based composite

Considering the results obtained in bare PG, the solidification step in samples containing EG was carried out at a slow cooling rate. Fig. 3

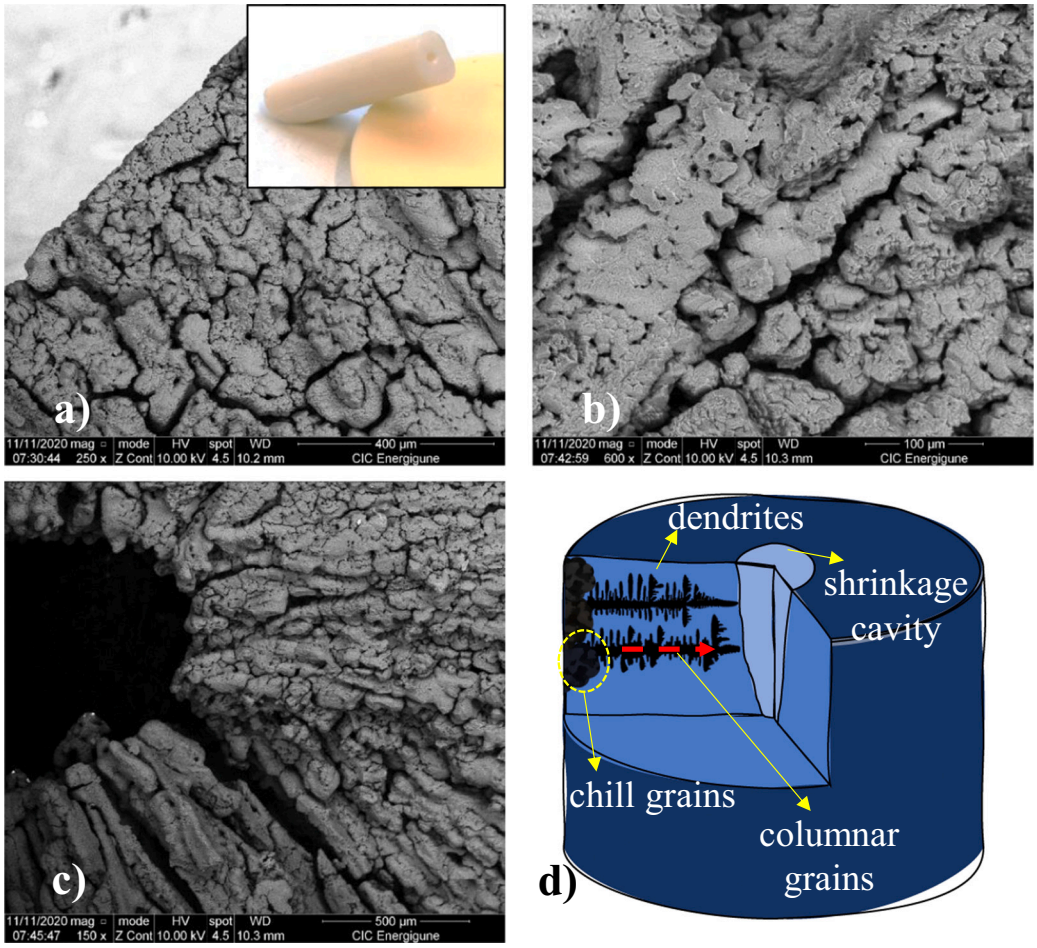

Fig. 1. a) Picture, SEM images along the axial axis (a. edge, b. medium and c. center) and structure scheme d) of cast PG processed at fast cooling rate.

shows the pictures of the obtained composites containing EG, processed both by casting and pressing. In casting, contents of EG higher than 5 wt % led to an excess of EG segregated from the PG. Therefore, composites containing 10 wt% of EG processed by casting were discarded. In contrast to casting, in uniaxial pressing, due to the pressure exerted on the axial axis of the pellets, the EG plates are aligned along the radial axis, with their surfaces resting on the horizontal plane. This alignment exposes a larger surface area of EG than in the case of casting, leading to a granite-like appearance overall in P_EG$_{600}$, with EG particles large enough to be visible with the unaided eye. On the other side, the smaller size of EG$_{75}$ causes a darker and more homogeneous aspect.

SEM images of the C_EG$_{75}$ and C_EG$_{600}$ series cross-sections are gathered in Fig. 4, representing the magnification that best shows the structure for a given composite. In addition, the brightness and contrast have been adjusted to make the presence of EG and its distribution more visible. From those images, it is noticeable that the EG is randomly distributed throughout the cross-section, generating homogenous composites. The most remarkable difference between these samples can be found in C5EG$_{75}$, where due to the smaller EG particle size, a 5 wt% addition results in a very homogeneous EG distribution that governs the whole microstructure, forming a continuous mesh of interconnected EG.

The SEM images of P_EG$_{75}$ and P_EG$_{600}$ series (Fig. 5) show the arrangement of the EG in the inner structure of the pellets. As can be seen in all images, it is confirmed that the EG plates tend to be aligned along the radial axis. For both series of samples, P_EG$_{75}$ and P_EG$_{600}$, the increase in graphite content promotes the formation of bonds between the EG plates, giving rise to interconnected graphite networks along the radial axis of the pellets. In this way, we move from having isolated EG plates for 1 % doping to a continuous EG network for 10 % doping. Concerning the graphite size used, the use of smaller EG (EG$_{75}$) favors the formation of a better distributed and more homogeneous interconnected network; on the contrary, when using EG$_{600}$, it is more likely to find areas of PG that limit the prolongation of the graphite network.

3.2. Bulk and true density

Table 1 provides the true and bulk densities of the obtained composites registered at room temperature.

Although EG exhibits a low apparent density, the true density is higher than that of PG (ca. 2.2 g/cm^3 [32]), therefore, as expected, the presence of EG, increases the true density of the composites in comparison with the bare PG specimens. It is noteworthy that in casting, the increase of the density with the EG incorporation is higher than in pressing (e.g., C5EG$_{75}$ and C5EG$_{600}$ vs. P5EG$_{75}$ and P5EG$_{600}$). In casting, by heating the sample to the melting point of the PG, the air trapped inside the EG sheets is evacuated, allowing the molten PG to embed itself inside the EG, filling the space previously occupied by air. This results in higher true densities, but it is also expected to lead to stronger PG-EG interaction. For the bulk density, it is observed a behavior contrary to the previous case, whereby the cast samples are less dense than those processed by pressing, reflecting the higher porosity of the cast composites. Fig. 6 shows the porosity of the composites calculated from Eq. (1). This figure evidences the difference in porosity between the samples obtained by casting and those obtained by pressing, mainly due to the shrinkage process that the former undergoes during solidification, which results in higher porosities. Furthermore, the significant effect that the addition of EG has on the reduction of porosity in the cast composites can be observed. The EG particles may be acting as

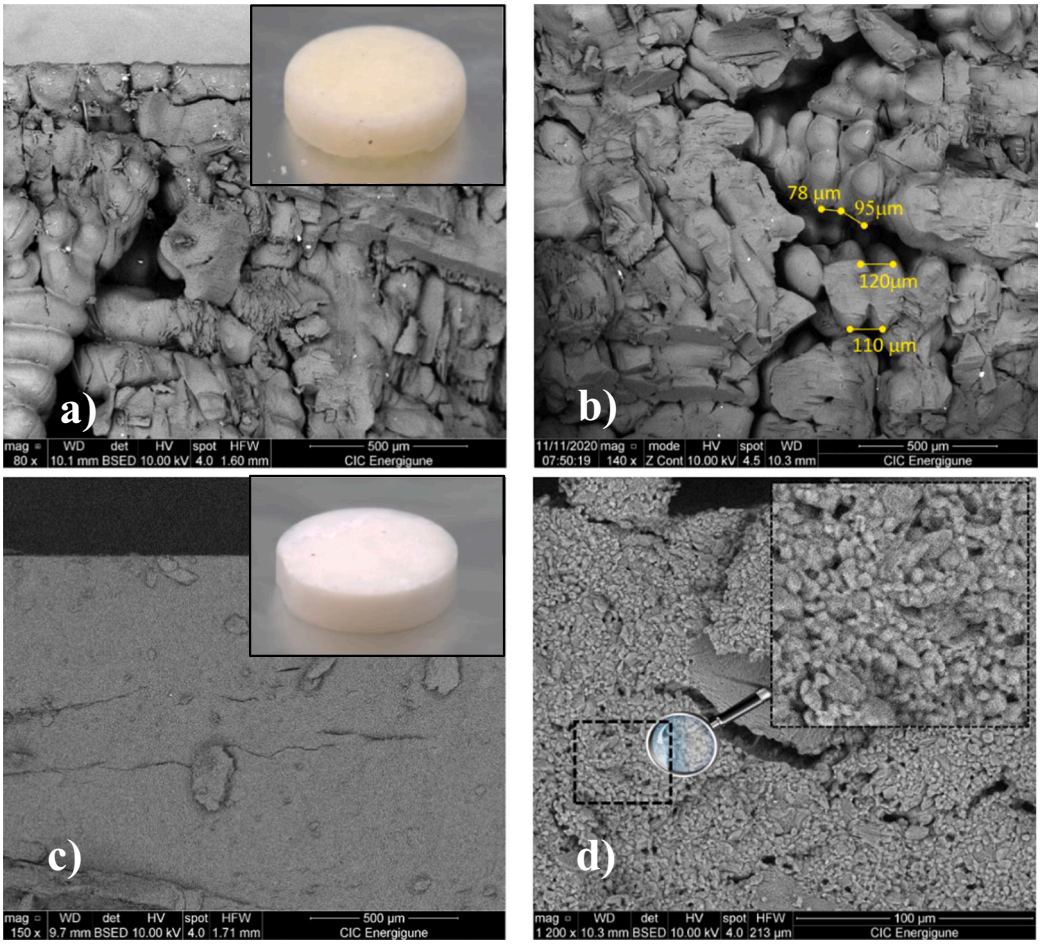

Fig. 2. a) Picture and SEM images of cast PG processed at slow cooling rate (a. edge and b. center); c) Picture and SEM images at different magnifications of PG processed by uniaxial pressing.

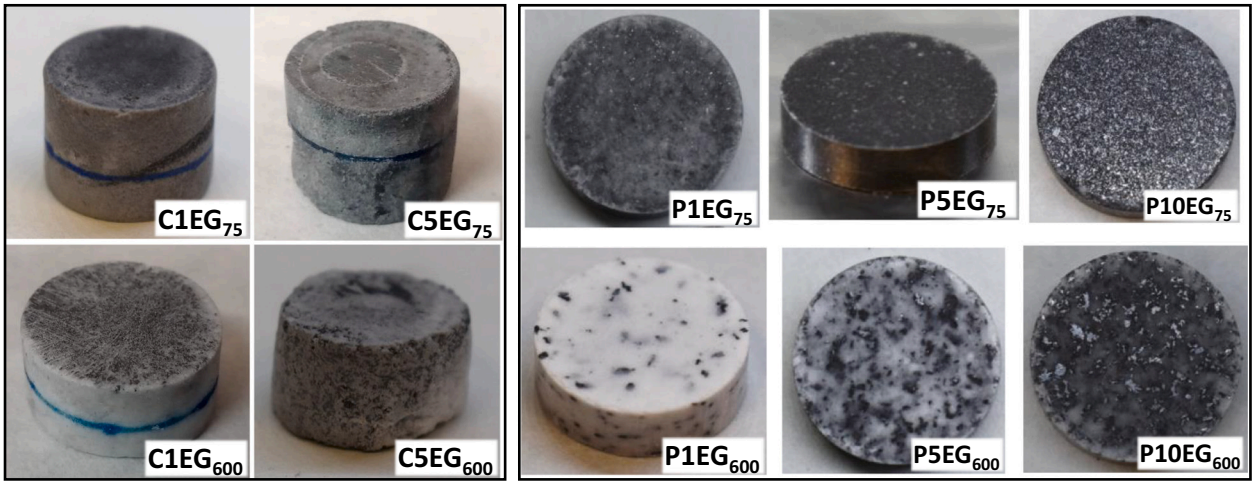

Fig. 3. Images C_EG$_{75}$ and C_EG$_{600}$ series (left); and images of P_EG$_{75}$ and P_EG$_{600}$ series (right).

nucleation sites, facilitating PG solidification without the need to undercool the molten PG, thus avoiding dendrite promotion, and reducing dendrite-derived porosity.

3.3. Mechanical properties

As a representative selection of the obtained composites, Fig. 7 depicts the strain-stress curves derived from compression tests both at room temperature (crystal phase) and at 120 °C (plastic phase) for the bare PG specimens.

As can be seen, in all cases, two regions of deformation are distinguished: an initial elastic deformation, in which stress and strain are proportional, followed by a permanent plastic deformation whose evolution depends on the current composite phase. The plastic deformation

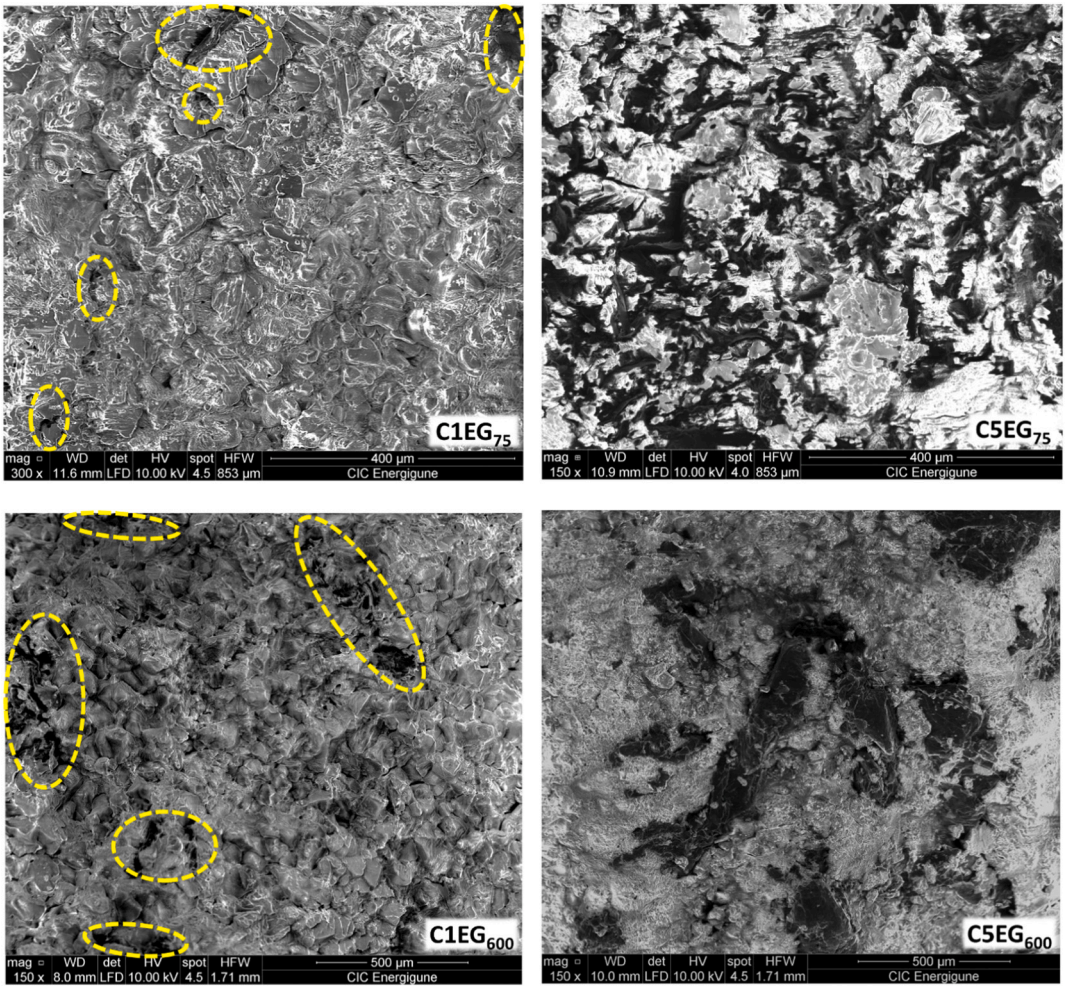

Fig. 4. SEM images of the inner structure of C_EG$_{600}$ and C_EG$_{75}$ series.

is very short for the crystal phase until fracture, showing brittle behavior. On the other hand, the long plastic deformation shows a ductile behavior in the plastic phase. Therefore, it evidences that the mechanism of this plastic deformation is different for crystal than for plastic phases. For the crystal phase, at room temperature, this deformation is accomplished by means of a process called slip, which involves the motion of dislocations, whereas plastic deformation in the plastic phase, at high temperature, occurs by a viscous flow mechanism [33,34]. Although for ease of understanding, only the strain-stress curves of pure PGs are shown in Fig. 7, the general behaviors previously discussed are also applicable to their composites containing EG.

The specific modulus (E*), which is the Young's modulus per mass density of a material, is calculated and plotted from strain-stress curves in Fig. 8. In general terms, the composites obtained by pressing have greater E* than their counterparts processed by casting. Elastic deformation depends on the interatomic bonding forces, therefore, microstructure characteristics like grain sizes do not affect E*. On the contrary, microscopic flaws or cracks have a noticeable impact on the composite behavior under applied stress. These flaws, which can be voids (porosity), inclusions, or sharp corners, act as an amplifier of the stress, decreasing E* [35,36]. Therefore, the higher porosity of cast composites promotes lower E* than the pressing ones. Furthermore, it can be observed that the incorporation of EG also decreases the specific modulus, indicating a lower Young's modulus value for the EG filler than for the PG matrix. Certainly, the low resistance to elastic deformation of expanded graphite, especially compared to other types of graphite, has been previously reported by several authors [37,38]. Thus, the modulus does not exceed 1.7 MPa for a EG density of 0.86 g/cm^3 [39], whereas it overcomes 200 MPa for 1.1 g/cm^3 [40], which agrees with the behavior observed in the composites. Hence, samples processed by pressing contain compressed EG, denser and with higher Young's modulus than those processed by casting [41].

When comparing the behavior for the different phases, composites in the plastic phase show a lower elastic modulus than in the crystal phase. As E* can be seen as a measure of the interatomic bonding forces, it was expected that the transition from the crystal to the plastic phase, which breaks hydrogen bonds, leads to a decrease also in the modulus of elasticity.

The yield point, that determines the elastic-plastic transition, obtained for the different composites both at the crystal and at plastic phases is shown in Fig. 9.

When analyzing the obtained yield point, it must be considered that this parameter is influenced by the grain size, the presence of EG, and the interaction between phases.

The grain size has a crucial effect on the mechanical strength of the composite. The grain boundary acts as a barrier to dislocation motion due to the different orientations of the two grains, hence, a dislocation passing through the boundary must change its direction of motion. Therefore, a fine-grained material with a greater total grain boundary area is harder than a coarse-grained one. Consequently, P0, with small grain sizes, exhibits a higher yield point than C0. This behavior is also observed when the materials are doped with EG. For the same EG content and processing, the obtained yield point is generally greater for EG$_{75}$, with larger grain boundary areas due to the smaller particle size,

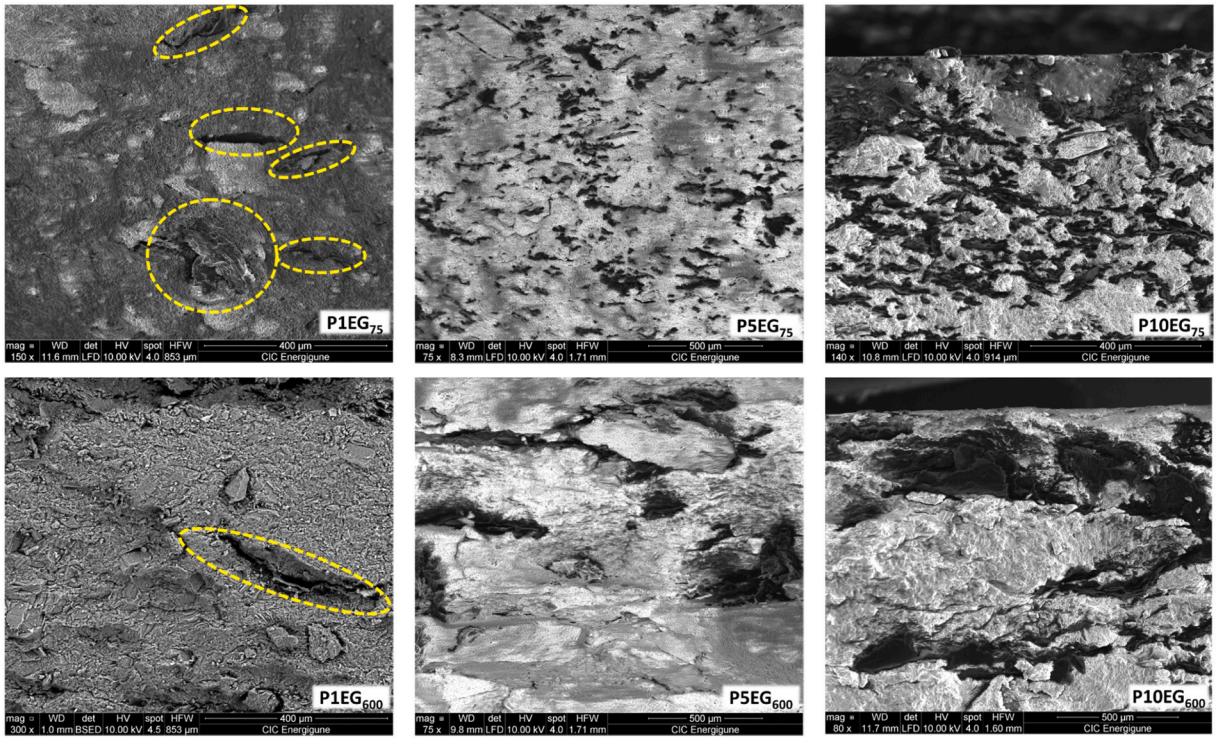

Fig. 5. SEM images of the inner structure of P_EG$_{75}$ and P_EG$_{600}$ series.

Table 1
True and bulk densities of the obtained composites as a function of the EG content and the processing method.

EG (%wt)	True density (g/cm^3)				Bulk density (g/cm^3)			
	P_EG$_{75}$	P_EG$_{600}$	C_EG$_{75}$	C_EG$_{600}$	P_EG$_{75}$	P_EG$_{600}$	C_EG$_{75}$	C_EG$_{600}$
0	1.188	1.188	1.230	1.230	1.155	1.155	1.019	1.019
1	1.238	1.241	1.232	1.233	1.174	1.193	1.068	1.011
5	1.231	1.231	1.273	1.261	1.186	1.185	1.135	1.085
10	1.262	1.269	–	–	1.224	1.216	–	–

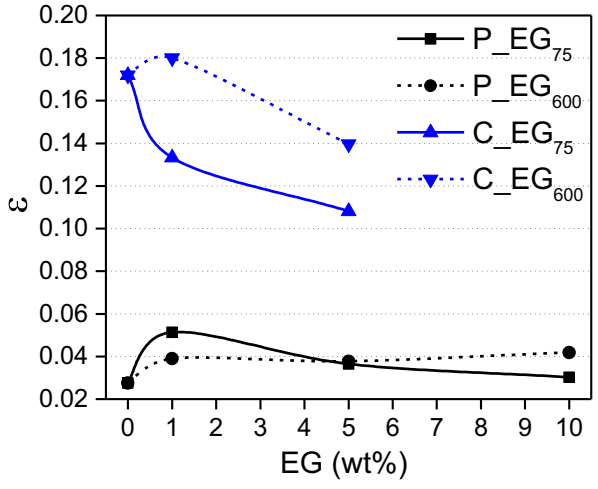

Fig. 6. Porosity (ε) of the processed composites.

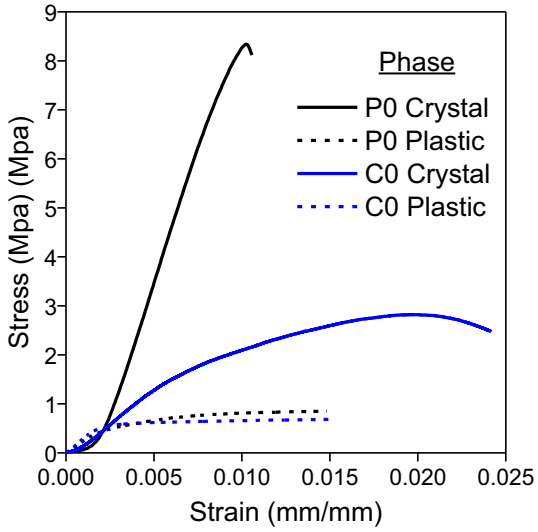

Fig. 7. Stress-strain curves under compression test for P0 and C0 at room temperature (crystal phase) and at 120 °C (plastic phase).

than for EG$_{600}$.

In addition to the microstructure, the degree of bonding between the matrix (PG) and the doping agent (EG) plays an important role. As previously commented, casting PG penetrates on the EG surface by viscous flow when it is melted, leading to certain mechanical bonding.

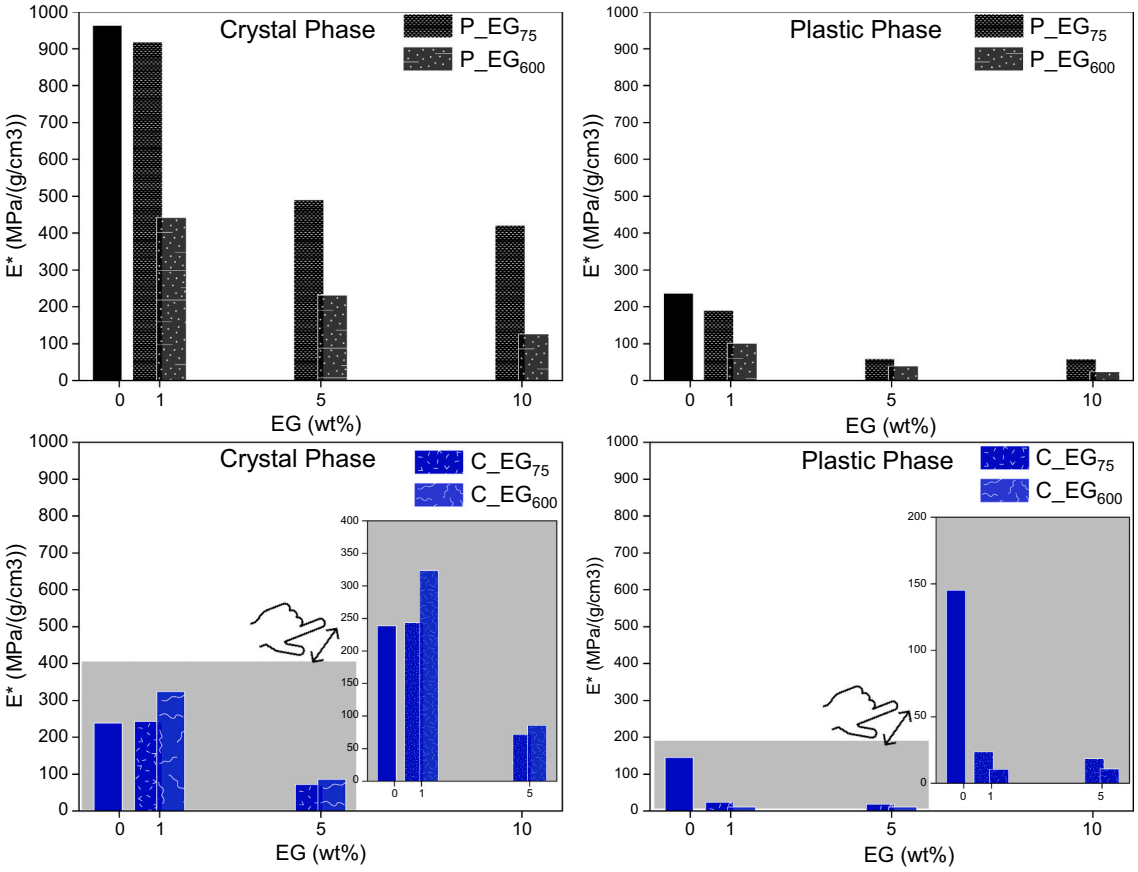

Fig. 8. Specific modulus of obtained composites. Black: pressing series; Blue: casting series. (Left: crystal phase; right: plastic phase). (For interpretation of the references to colour in this figure legend, the reader is referred to the web version of this article.)

This greater PG-EG interphase interaction leads to higher mechanical resistance when adding EG to cast composites. This is especially evident at EG contents of 5 wt%, where the PG-EG interaction becomes noticeable.

3.4. Thermal expansion

One of the important properties of materials intended for thermal storage is their thermal expansion, especially if they are stacked or coated in the final application. To evaluate this property, three heating/cooling cycles have been performed in a dilatometer to record the thermal expansion of the composites. To better understand the effect of processing on thermal expansion, Fig. 10 compares the second cycle of C0, P0, and P5EG$_{75}$. We display only P5EG$_{75}$, but the general behavior observed in the graph can be extended to any of the samples containing EG (pressing series).

In these tests, an unexpected behavior was observed in casting samples (C_EG$_{75}$ and C_EG$_{600}$ series). The samples produced by casting cracked during the dilatometry test, probably due to excessive expansion of the air contained in their pores during heating. As a prelude of what would happen with the series of samples C_EG$_{75}$ and C_EG$_{600}$, in Fig. 10, in red, a sudden thermal expansion can be observed in C0 during the phase transition, while its contraction is smaller compared to P0 and P5EG$_{75}$. Due to the failure of samples C_EG$_{75}$ and C_EG$_{600}$, the data recorded in the dilatometry test for these samples are not considered reliable. Nevertheless, it is evident that casting processing has a negative effect on the mechanical stability of the specimens during thermal cycling. About the samples obtained by pressing, the expansion experienced during heating is greater than the thermal contraction on cooling, leading to a permanent deformation of the material. Nevertheless, in P5EG$_{75}$ the presence of EG facilitates the contraction during the phase transition on cooling, as can be seen in the abrupt change of slope during the plastic-crystal transition.

In addition to the thermal expansion, relevant information about the phase transitions of the composites can be extracted from the dilatometry tests. An approximation of the beginning and end phase transition temperature can be obtained from the intersection of the lines that fit each expansion/contraction section. Although these values do not serve as a reference for precise real values, they serve to compare the behavior between samples. In this way, the degree of subcooling of these composites can be obtained, which is a critical parameter when dealing with materials intended for thermal energy storage. Table 2 shows the subcooling observed during dilatometry for the different composites tested. These values show a decrease in subcooling in specimens processed by pressing, being the subcooling degree between 3.5 and 6.8 °C, meanwhile, C0 exhibits 8.1 °C of hysteresis. This behavior was confirmed by DSC (Fig. 10, upper left corner). This is not a minor observation since, in the literature reported to date, the PG subcooling is found to be between 8 °C to 13 °C [7,20,21]. A significant reduction of this hysteresis in solid-solid PCMs has not yet been reported, and it would help to deal with one of the major obstacles of these materials for their successful entry into the energy market. Although we want to record this observation, the thermal behavior of these materials will be studied in future work.

From the slope of each section, we can obtain the corresponding linear expansion coefficient. Fig. 11 gathers the linear expansion coefficients (obtained from the second cycle) for the crystal phase, phase transition, and plastic phase, both during heating and cooling. It is observed that the linear expansion coefficients in contraction are smaller than the ones registered during expansion in each of the sections, leading to permanent deformations. However, the presence of expanded

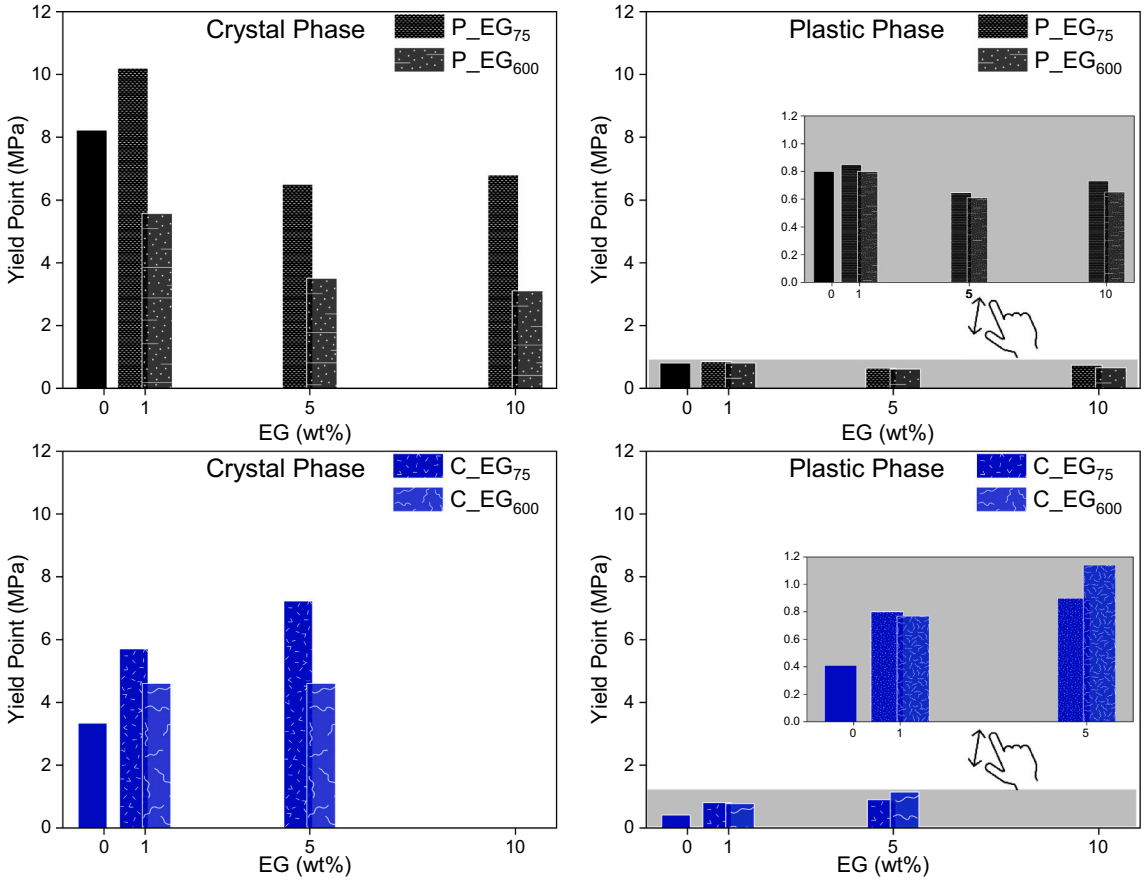

Fig. 9. Yield point (MPa) of obtained composites. Black: pressing series; Blue: casting series. (Left: crystal phase; right: plastic phase). (For interpretation of the references to colour in this figure legend, the reader is referred to the web version of this article.)

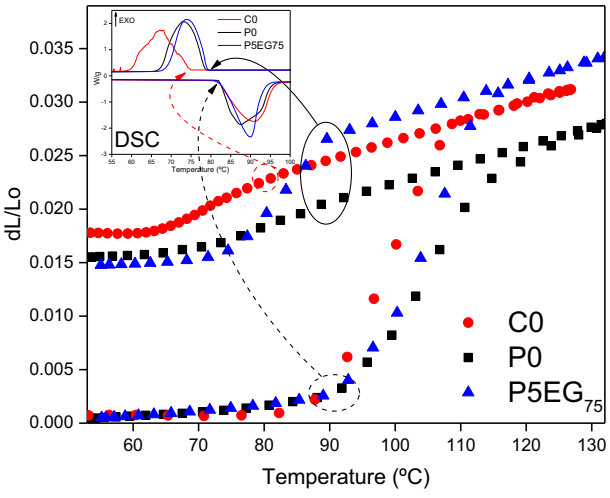

Fig. 10. Second cycle of thermal expansion/contraction.

Table 2
Subcooling degree observed in dilatometry test.

EG content (wt%)	P_EG_{75}	P_EG_{600}	Casting
	ΔT (°C)		
0	3.57	3.57	8.08
1	6.77	4.56	–
5	4.06	5.62	–
10	4.31	4.19	–

graphite retains the expansion in the plastic phase, allowing similar contraction-expansion coefficients as the EG content increases. To examine this behavior, we analyze 10 additional thermal cycles (Fig. 11. b) for the most extreme cases, P0 and $P10EG_{75}$, which present the largest and the smallest difference between their expansion/contraction coefficients, respectively. As expected, P0 undergoes a greater deformation in the first cycles. This deformation reached its limit from the 4th cycle onwards, and no further changes were recorded. After the test, P0 had increased in diameter and lost its initial shape stability, crumbling easily when handled. On the other hand, although the deformation of $P10EG_{75}$ is initially more moderate, this deformation does not cease after 13 cycles. The extension of this deformation diminishes with the number of cycles, deviating progressively from the linear trend marked by the gray line in the graph. Hence, it is expected that, after several successive cycles, $P10EG_{75}$ will reach a deformation limit similar to that observed in P0, also losing its shape stability. After the test, $P10EG_{75}$ only deformed along its axial axis, presenting the same initial diameter (8.00 mm). This behavior reflects the EG effect, which completely retains the deformation along the axis along which it is aligned.

Finally, considering the behavior of the material as isotropic, a situation that could be applied to undoped compounds as P0, the volumetric expansion coefficient (γ) can be obtained as the product of 3 times the coefficient of linear expansion (α) [42]. With this coefficient, the volumetric expansion that the material undergoes during the phase transition can be estimated. Thus, P0 composite presents a volumetric expansion of 6.23 %, a value in the range of those previously reported for the transition in NPG (4.9 %) [43,44] and in PG itself (5.4 %) [45]. It is noted that this volume change is much smaller than that typically shown for solid-liquid PCMs (12–15 %). This volumetric expansion would be even smaller in the case of EG doping, as it introduces a

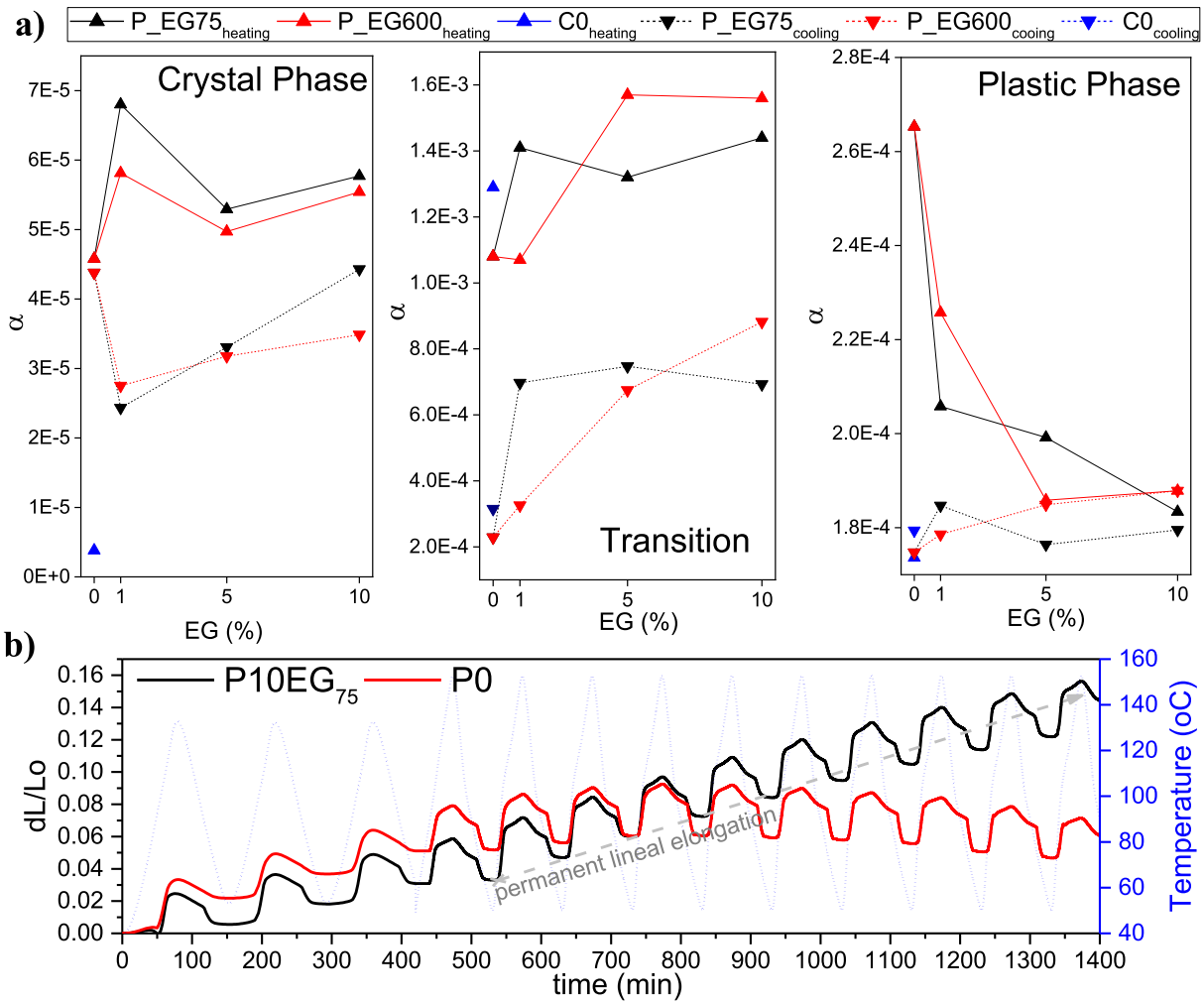

Fig. 11. a) Coefficients of thermal expansion for crystal, transition and plastic phases registered during the second cycle of heating/cooling in the dilatometry test. b) Thermal expansion during thermal cycling. From the 3rd cycle, the heating/cooling rate was increased to 2 °C/min to accelerate the analysis.

mechanical constraint to the matrix expansion. This lower volumetric change would facilitate the application of coatings or encapsulants to cope with the demanding operating conditions. It must be mentioned that the deformation of these materials and their volumetric change, although small, could cause overpressures if they are confined in a coating. It is well known that under certain pressures plastic crystals show barocaloric effects that shift their transition temperatures, however, the pressures necessary for these effects to appear are so huge that they are not expected to occur in these cases [43].

4. Conclusions

The effect of processing on the structure of pentaglycerine-based composites containing EG has been explored. It was observed that casting produces pieces with greater porosity than the pressing ones and leads to a random distribution of the dopant particles. On the other hand, pressing leads to an EG arrangement aligned along the radial axis. Moreover, cast composites exhibit higher PG-EG interaction due to the inoculation of the molten PG inside the EG during the casting process. This microstructure influences the mechanical properties. Hence, in the crystal phase, composites are brittle, and the porosity and the addition of EG decrease their mechanical resistance, which is more pronounced in castings. On the contrary, in the plastic phase, the plastic deformation under compression occurs by a viscous flow mechanism. In that scenario, the greater PG-EG interphase interaction leads to higher mechanical resistance when adding EG to cast composites.

Regarding thermal expansion, for all the samples, as cycles are performed, there is a permanent deformation in the piece. However, the presence of expanded graphite influences the plastic phase, allowing similar contraction-expansion coefficients. These deformations could be critical when the materials are stacked in a tank, so they need an additional coating or filler to mitigate this deformation. Therefore, future studies must focus on avoiding deformation, testing the effect of different filler geometries, applying retention coatings, and evaluating the mechanical properties in conjunction with the filler and the coating. On the other hand, the volume change observed during the transition (<6.8 %) is smaller than that typically shown for solid-liquid PCMs (12–15 %). This volumetric expansion is even smaller in the case of EG doping.

Finally, composites manufactured by pressing showed considerably less subcooling than those processed by casting. This significant reduction in subcooling of plastic crystals has not been previously reported, and it would help to deal with one of the main obstacles of these materials for their successful entry into the energy market. Therefore, future research is needed to elucidate the causes behind this subcooling reduction, as well as to complete and extend the understanding of the processing effect on the main thermophysical properties of PG/EG-based composites (latent heat, subcooling, thermal conductivity and transition kinetics).

CRediT authorship contribution statement

Ángel Serrano: Conceptualization, methodology, formal analysis, investigation, resources, data curation, writing-original draft preparation, writing-review and editing, visualization. **Ignacio Garrido**: methodology, validation, formal analysis, investigation, data curation. **Sergio Santos**: formal analysis, investigation, data curation. **Mikel Duran**: formal analysis, investigation, data curation. **Jean-Luc Dauvergne**: software, investigation, data curation, resources, writing-review and editing **Manuel Carmona**: writing-review and editing. **Elena Palomo Del Barrio**: conceptualization, writing-review and editing-supervision, Project administration, funding acquisition.

Declaration of competing interest

The authors declare that they have no known competing financial interests or personal relationships that could have appeared to influence the work reported in this paper.

Data availability

Data will be made available on request.

Acknowledgment

This research was funded by the FEDER/Ministerio de Ciencia e Innovación–Agencia Estatal de Investigación, SWEET-TES project (RTI2018-099557-B-C21), as well as from The Basque Government (Elkartek CICe2020, KK-2020/00078). The authors also gratefully acknowledge Yagmur Polat and Cristina Luengo for their technical support.

References

[1] Z. Li, Y. Lu, R. Huang, J. Chang, X. Yu, R. Jiang, X. Yu, A.P. Roskilly, Applications and technological challenges for heat recovery, storage and utilisation with latent thermal energy storage, Appl. Energy 283 (2021), 116277, https://doi.org/10.1016/J.APENERGY.2020.116277.

[2] A. Serrano, M. Duran, J.L. Dauvergne, S. Doppiu, E.P. Del Barrio, Tailored transition temperature plastic crystals with enhanced thermal energy storage capacity, Sol. Energy Mater. Sol. Cells 220 (2021), 110848, https://doi.org/10.1016/j.solmat.2020.110848.

[3] A. Serrano, J.-L. Dauvergne, S. Doppiu, E. Palomo Del Barrio, Neopentyl glycol as active supporting media in shape-stabilized PCMs, 2019, https://doi.org/10.3390/ma12193169.

[4] S. Santos-Moreno, S. Doppiu, G.A. Lopez, N. Marinova, Á. Serrano, E. Silveira, E. P. del Barrio, Study of the phase transitions in the binary system NPG-TRIS for thermal energy storage applications, Materials (2020), https://doi.org/10.3390/ma13051162 (Basel).

[5] K.P. Venkitaraj, S. Suresh, B. Praveen, Experimental charging and discharging performance of alumina enhanced pentaerythritol using a shell and tube TES system, Sustain. Cities Soc. 51 (2019), 101767, https://doi.org/10.1016/J.SCS.2019.101767.

[6] K.P. Venkitaraj, S. Suresh, B. Praveen, Energy storage performance of pentaerythritol blended with indium in exhaust heat recovery application, Thermochim. Acta 680 (2019), 178343, https://doi.org/10.1016/J.TCA.2019.178343.

[7] M. Barrio, J. Font, J. Muntasell, J. Navarro, J.L. Tamarit, Applicability for heat storage of binary systems of neopentylglycol, pentaglycerine and pentaerythritol: a comparative analysis, Sol. Energy Mater. 18 (1988) 109–115, https://doi.org/10.1016/0165-1633(88)90051-2.

[8] D.K. Benson, J.D. Webb, R.W. Burrows, J.D.O. McFadden, C. Christensen, Materials Research for Passive Solar Systems: Solid-state Phase-change Materials, Solar Energy Research Inst, Golden, CO (USA), 1985.

[9] J. Muntasell, M. Barrio, J. Font, D.O. López, J.L. Tamarit, M.A.C. Diarte, J. Guion, M. Teisseire, N.B. Chanh, Y. Haget, Plastic crystals and their potential use in new technologies, J. Therm. Anal. 3710 (37) (1991) 2395–2398, https://doi.org/10.1007/BF01913741.

[10] H. Feng, X. Liu, S. He, K. Wu, J. Zhang, Studies on solid-solid phase transitions of polyols by infrared spectroscopy, Thermochim. Acta (2000), https://doi.org/10.1016/s0040-6031(99)00403-7.

[11] D. Chandra, W.M. Chien, V. Gandikotta, D.W. Lindle, Heat capacities of "Plastic Crystal" solid state thermal energy storage materials, Z.Phys. Chem. 216 (2002) 1433, https://doi.org/10.1524/ZPCH.2002.216.12.1433/MACHINEREADABLECITATION/RIS.

[12] A. Mishra, A. Talekar, D. Chandra, W.M. Chien, Ternary phase diagram calculations of pentaerythritol-pentaglycerine- neopentylglycol system, Thermochim. Acta (2012), https://doi.org/10.1016/j.tca.2012.02.009.

[13] R. Shi, D. Chandra, A. Mishra, A. Talekar, M. Tirumala, D.J. Nelson, Thermodynamic reassessment of the novel solid-state thermal energy storage materials: ternary polyalcohol and amine system pentaglycerine-tris (hydroxymethyl)-amino-methane-neopentylglycol (PG-TRIS-NPG), Calphad (2017), https://doi.org/10.1016/j.calphad.2017.08.003.

[14] M. Barrio, D.O. López, J.L. Tamarit, P. Negrier, Y. Haget, Molecular interactions and packing in molecular alloys between nonisomorphous plastic phases, J. Solid State Chem. 124 (1996) 29–38, https://doi.org/10.1006/JSSC.1996.0203.

[15] H. Singh, An experimental phase diagram study of ternary pentaerythritol-pentaglycerine-neopentylglycol orieintationally disordered plastic crystals, 2011.

[16] V.K. P, S. Suresh, B. Praveen, A. Venugopal, S.C. Nair, Pentaerythritol with alumina nano additives for thermal energy storage applications, J. Energy Storage 13 (2017) 359–377, https://doi.org/10.1016/J.EST.2017.08.002.

[17] K.P. Venkitaraj, S. Suresh, Experimental thermal degradation analysis of pentaerythritol with alumina nano additives for thermal energy storage application, J. Energy Storage 22 (2019) 8–16, https://doi.org/10.1016/J.EST.2019.01.017.

[18] D. Mani, M.K. Saranprabhu, K.S. Rajan, Intensification of thermal energy storage using copper-pentaerythritol nanocomposites for renewable energy utilization, Renew. Energy 163 (2021) 625–634, https://doi.org/10.1016/J.RENENE.2020.08.119.

[19] T. Liu, Q. Yang, X. Gong, L. Wang, E. Yao, H. Zou, Investigation on thermal conductivities of pentaerythritol-graphene composites for thermal energy storage, Heat Mass Transf. 57 (2021) 1909–1919, https://doi.org/10.1007/S00231-021-03076-Z/FIGURES/9. Und Stoffuebertragung.

[20] D.J. Johnson, J.S. Ervin, M. Hanchak, S.S. Patnaik, X. Hu, in: Graphite foam infused with pentaglycerine for solid-state thermal energy storage 29, 2015, pp. 55–64, https://doi.org/10.2514/1.T4484.

[21] N. Zhang, Y. Song, Y. Du, Y. Yuan, G. Xiao, Y. Gui, A novel solid-solid phase change material: pentaglycerine/expanded graphite composite PCMs, Adv. Eng. Mater. 20 (2018) 1800237, https://doi.org/10.1002/ADEM.201800237.

[22] J. Wang, G. Chen, H. Jiang, Theoretical study on a novel phase change process, Int. J. Energy Res. (1999), https://doi.org/10.1002/(SICI)1099-114X(19990325)23:4<287::AID-ER476>3.0.CO;2-K.

[23] M.M. Kenisarin, K.M. Kenisarina, Form-stable phase change materials for thermal energy storage, Renew. Sustain. Energy Rev. (2012), https://doi.org/10.1016/j.rser.2012.01.015.

[24] A. Fallahi, G. Guldentops, M. Tao, S. Granados-Focil, S. Van Dessel, Review on solid-solid phase change materials for thermal energy storage: molecular structure and thermal properties, Appl. Therm. Eng. (2017), https://doi.org/10.1016/j.applthermaleng.2017.08.161.

[25] T. Nomura, N. Okinaka, T. Akiyama, Technology of latent heat storage for high temperature application: a review, ISIJ Int. 50 (2010) 1229–1239, https://doi.org/10.2355/ISIJINTERNATIONAL.50.1229.

[26] X. Du, H. Wang, Y. Wu, Z. Du, X. Cheng, Solid–solid phase-change materials based on hyperbranched polyurethane for thermal energy storage, J. Appl. Polym. Sci. 134 (2017) 45014, https://doi.org/10.1002/APP.45014.

[27] W. Lovejoy, S. Fixson, S. Jackson, Product Costing Guidelines, 2005.

[28] W.D. Callister, D.G. Rethwisch, in: William D. Callister, David G. Rethwisch (Eds.), Materials Science And Engineering, Wiley, 2011.

[29] C.T. Rueden, J. Schindelin, M.C. Hiner, B.E. DeZonia, A.E. Walter, E.T. Arena, K. W. Eliceiri, Image J2: ImageJ for the next generation of scientific image data, BMC Bioinform. (2017), https://doi.org/10.1186/s12859-017-1934-z.

[30] H. Abrams, Grain size measurement by the intercept method, Metallography 4 (1971) 59–78, https://doi.org/10.1016/0026-0800(71)90005-X.

[31] D.R. Askeland, P.P. Fulay, W.J. Wright, Ciencia e ingeniería de materiales, Cengage learning, 2017.

[32] Expandable Flake Graphite, Asbury carbons (n.d.), https://asbury.com/es/recursos/education/science-of-graphite/expandable-flake-graphite/. (Accessed 29 May 2022).

[33] O.D. Sherby, O.A. Ruano, J. Wadsworth, Deformation Mechanisms in Crystalline Solids And Newtonian Viscous Behavior, Lawrence Livermore National Lab.(LLNL), Livermore, CA (United States), 1999.

[34] G. Yang, S.J. Park, Deformation of single crystals, polycrystalline materials, and thin films: a review, Materials 12 (2019) 2003, https://doi.org/10.3390/MA12122003.

[35] J. Kováčik, Correlation between Young's modulus and porosity in porous materials, J. Mater. Sci. Lett. 18 (1999) 1007–1010.

[36] J.C. Wang, Young's modulus of porous materials, J. Mater. Sci. 193 (19) (1984) 801–808, https://doi.org/10.1007/BF00540451.

[37] E. Solfiti, F. Berto, Mechanical properties of flexible graphite, Procedia Struct. Integr. 25 (2020) 420–429.

[38] P. Jaszak, Adaptation of a highly compressible elastomeric material model to simulate compressed expanded graphite and its application in the optimization of a graphite-metallic structure, J. Braz.Soc. Mech. Sci. Eng. 42 (2020) 1–22.

[39] P.-H. Chen, D.D.L. Chung, Elastomeric behavior of exfoliated graphite, as shown by instrumented indentation testing, Carbon N. Y. 81 (2015) 505–513.

[40] M. Khelifa, V. Fierro, J. Macutkevič, A. Celzard, Nanoindentation of flexible graphite: yxperimental versus simulation studies, Adv. Mater. Sci. 3 (2018) 1–11.

[41] R. Goudarzi, G. Hashemi Motlagh, Relationship between pore structure with residual pore and mechanical properties of expanded graphite nanocomposites at varying molding pressures, J. Appl. Polym. Sci. 138 (2021) 50994.

[42] R.A. Schapery, Thermal expansion coefficients of composite materials based on energy principles, J. Compos. Mater. 2 (1968) 380–404.
[43] P. Lloveras, A. Aznar, M. Barrio, P. Negrier, C. Popescu, A. Planes, L. Mañosa, E. Stern-Taulats, A. Avramenko, N.D. Mathur, Colossal barocaloric effects near room temperature in plastic crystals of neopentylglycol, Nat. Commun. 10 (2019) 1–7.
[44] M. Barrio, J. Font, D.O. López, J. Muntasell, J.L. Tamarit, Y. Haget, Thermal-expansion tensors of pentaerythritol (PE) and pentaglycerin (PG) and compositional deformation tensor of PG1− xPEx molecular alloys, J. Appl. Crystallogr. 27 (1994) 527–531.
[45] J. Font, J. Muntasell, E. Cesari, Plastic crystals: dilatometric and thermobarometric complementary studies, Mater. Res. Bull. 30 (1995) 839–844.